PCCP

Accepted Manuscript

ROYAL SOCIETY OF CHEMISTRY

www.rsc.org/pccp

Time-gated pre-resonant femtosecond stimulated Raman spectroscopy of diethylthiatricarbocyanine iodide

Hyung Min Kim[⊥,a], Hyunmin Kim[⊥,b], Ilseung Yang[c], Seung Min Jin[c,d,*], Yung Doug Suh[d,f,*]

[a]*Department of Bio & Nano Chemistry, Kookmin University, Seoul 136-702, Republic of Korea*

[b]*Nano Bio Research Division, Daegu Gyeongbuk Institute of Science and Technology, Daegu 711-873, Republic of Korea*

[c]*iiSM Inc. 141 Gajeongro, Yuseong-gu, Daejeon 305-600, Republic of Korea*

[d]*Laboratory for Advanced Molecular Probing (LAMP), Research Center for Convergence Nanotechnology, Korea Research Institute of Chemical Technology, DaeJeon 305-600, Republic of Korea*

[f]*School of Chemical Engineering, Sungkyunkwan University, Suwon 440-746, Repiblic of Korea*

[⊥] These authors contributed equally to this article. *corresponds to smjin@krict.re.kr, ydsuh@krict.re.kr

Fax: +82-42-860-7625; Tel: +82-42-860-7597

ABSTRACT

We present time-gated femtosecond stimulated Raman spectroscopy (fSRS) in the pre-resonance Raman condition of diethylthiatricarbocyanine (DTTC) iodide. A 'pseudo emission-free' condition is achieved by delivering the probe beam ahead of the pump beam. Regeneratively amplified pulse trains are employed to create an angle-geometry (non-collimated) mixing between the pump and probe beams, leading to highly sensitive measurement of the stimulated Raman gain. Time-integrated spectroscopy allows for a more quantitative distinction between the contributions of stimulated Raman scattering and stimulated emission. We successfully obtain a highly sensitive (signal-to-noise ratio > 100) stimulated Raman spectrum in the optimized condition, which compares favourably to results

obtained with two-dimensional correlation spectroscopy (2DCOS). Given the optical pre-resonance of ~0.1 eV, the background signals mostly originate from the stimulated emission of excited electrons and are significantly reduced by partial overlapping of the pump and probe beams; a genuine fSRS spectral profile is obtained for a temporal delay of ~0.2 ps between the two beams.

1. INTRODUCTION

Stimulated Raman scattering (SRS) is becoming more prevalent as researchers recognise its excellent characteristics: the linearity of the responding signal and the suppression of non-vibrationally induced responses.[1] SRS spectroscopy was initially developed to improve the low scattering efficiency of Raman scattering spectroscopy (approximately one event in a million photonic excitations) with intense lasers in the 1960s.[2] SRS occurs when two optical pulses coherently excite a molecule, allowing synchronized energy transfer between the photons and molecule through light–matter interactions.[3] Optical coherency is obtained when the optical frequencies of the excitation beams differ by an amount equal to the target vibrational frequency of the molecule, as in other coherent Raman scattering techniques such as coherent anti-Stokes Raman scattering (CARS).[4] However, optical coherency in SRS can also be simultaneously achieved for multiple vibrational states by allowing the mixing of short (femtosecond) and long (picosecond) pulses, which is known as femto-stimulated Raman scattering (fSRS).[5] This type of SRS is advantageous for time-spectral profiles in small uncertainty principle region (<500 fs·cm^{-1})[6] and has been employed extensively for investigations of chemical reaction dynamics,[7] vibrational structural changes,[8] and time evolution of molecular isomerization.[9]

Since its introduction in 1970,[10] resonant Raman spectroscopy has played a pivotal role in providing physiochemical descriptions of excited state dynamics attributed to large signal

enhancements associated with the scattering cross section of the resonance, which is ~10^6 times larger than that of the off-resonance Raman condition.[11] However, the intense fluorescence background and subsequent weak resolvable Raman signals limit the applications of 'spontaneous' resonance Raman spectroscopy. Suppressing undesirable fluorescence interference has been achieved in a number of studies by, for example, Fourier filtering,[12] interferometric measurements,[13] Kerr-gatings,[14] and fSRS. In the case of fSRS, the Mathies Lab at the University of California has pioneered the adoption of the dispersive nature of resonance fSRS for analysis purposes, addressing negative (stimulated Raman loss; SRL) and positive (stimulated Raman gain; SRG) features in fSRS spectra. Their studies have suggested that optimal conditions for rejecting the fluorescence background can be obtained by slightly tuning off the wavelength of the excitation beam from the exact position of the electronic absorption.[15,16] The SRG is expressed as:

$$\mathrm{SRG} \propto \mathrm{N} \times \left(\frac{\partial^2\sigma}{\partial\omega\partial\Omega}\right)_0 \times I_{pump} \times I_{Probe} \quad (1)$$

where N is the number of the molecules, $\left(\frac{\partial^2\sigma}{\partial\omega\partial\Omega}\right)_0$ is a spontaneous differential Raman cross-section, and I_{pump} and I_{probe} are the beam intensities of the pump and probe pulses, respectively.[17] In practice, the SRG is determined from the change in the probe field by subtracting the beam intensity in the presence and absence of the pump field, which drastically diminishes the non-vibrationally contributed resonance terms. In addition, the fluorescence background signals are minimized by employing a detector with a small collection angle. Thus, stimulated emission (STE) by coherently grounding electrons from the excited states remains the main obstacle in improving the spectral resolution in resonance fSRS spectroscopy.

Time-gated measurements are an important tool for reducing background signals in nonlinear optical fluorescence and vibrational spectroscopy. Recently, Vicidomini *et al.*[18] achieved a sub-50-nm-scale resolution in stimulated emission depletion (STED) microscopy by monitoring the fluorescence using the time-gated approach. Using a pulsed (~150 ps) beam combined with a continuous wave (cw) STED beam, they detected fluorescence signals delayed by tens of

nanoseconds (10–20 ns) and revealed the membrane structure of a living cell at a resolution below the diffraction limit with a STED beam of a moderate power (<100 mW). This result has also been confirmed by theoretical calculations for cw- and pulsed-STED beams.[19] In coherent Raman spectroscopy (CRS), the non-resonant background originating from the virtual-state-related electronic transitions are problematic. Solutions have been sought in frequency modulation,[20] heterodyne detection,[21] and time-gated measurement.[22] Pestov *et al.*[23] reported background-suppressed CARS spectroscopy using a time-gated approach and a three-wave mixing (pump–Stokes–probe) method. They retrieved highly species-specific and background-free spectra for marker molecules of bacterial endospores by delaying the timing of the probe mixing by ~1.5 ps from the moment of synchronization of the pump and Stokes beams. The short lifetime (~1 ps) of the non-resonant CARS signal permitted the almost complete removal of the background.

In contrast to off-resonant CRS spectroscopy, background signals from resonant fluoropores in fSRS spectroscopy are strongly correlated to the STE. Because the fluorescence lifetime (>10 ps) is longer than that of non-resonant CRS signals (~1 ps), carrying out time-gated detection by *delaying* the overlap time of the probe beam with respect to the pump beam to eliminate the background signal is not feasible. We discuss here an alternative time-gated fSRS spectroscopy that does not require a post-data-processing step to achieve a background-free Raman spectrum. More specifically, we exploit broadband fSRS spectroscopy based on a *probe-ahead* time-gated technique to reveal details of the chemical structure of diethylthiatricarbocyanine (DTTC) iodide molecules in the resonant Raman condition without the disturbance of STE.

2. EXPERIMENTAL

An outline of our fSRS system, which consists of a femtosecond laser and a detection system, is presented graphically in Fig. 1(A). The source-laser pulse (800 nm, 130 fs, 1 W) is provided by a regenerative amplifier system (Spectra-Physics, Spitfire Pro F) operating at 1

kHz that is seeded by an ultrafast femtosecond Ti:Sapphire oscillator (Spectra-Physics, MaiTai SP) at an 80-MHz repetition rate. The source beam is divided by an 80:20 beam splitter (CVI Melles Griot, BS1-800-80-1012-45P) with the larger portion (80%) of the output adopted as the Raman pump and the remainder (20%) is focused on to a 1-mm-thick sapphire plate (Newport, SAW25) to provide a supercontinuum probe light. Gold-coated concave mirrors serve as collimating and focusing elements for the supercontinuum beam to avoid any dispersion in the group velocity. The supercontinuum beam then passes through a 50:50 broadband beam splitter to create the reference beam and Raman probe. Since the spectral resolution of fSRS is determined by the full width at half maximum (FWHM) of the Raman pump pulse (*i.e.*, the longer pulse),[6] we direct this beam through a narrow spectral bandpass filter (Andover, 010FC14-25) to achieve a resolution of ~1 nm.

The temporal delay between the pump and probe beams is controlled by a motorized translation stage (Parker Hannifin Co., Daedal, 400LXR). After passing through the sample placed in a 10-mm-long cuvette, the Raman probe is filtered through a holographic notch filter (Kaiser, customized for 800 nm) and a glass colour filter (CVI Melles Griot, RG-1000/RG-830) to purify the spectrum in the range of interest by attenuating the high-intensity pump and unwanted probe beams, respectively. An iris is also employed to block the intensity of the pump beam under angled-beam mixing geometry conditions. The Raman probe is then incident on an optical fibre or directly focused into the polychromator (Princeton Instruments, SP 2300i) that is attached to a charge-coupled device (CCD) system (Acton, Pixis-400BR). At the same time, the reference beam is recorded to compensate for pulse-power fluctuations and is subject to the same filtration (notch/colour) steps as the probe beam to extract the difference induced by the sample. The recorded spectra are processed computationally using Labview software written in-house to obtain the net SRG, defined experimentally as:

$$\mathrm{SRG} = ln\frac{(\Delta I_{probe} \div \Delta I_{reference})_{pump\ on}}{(\Delta I_{probe} \div \Delta I_{reference})_{pump\ off}} \quad (2)$$

where ΔI is the signal intensity after subtraction of the CCD noise. We do not optically block the pump beam in the pump-off condition but instead allow the probe beam to pass ahead of the pump beam by several picoseconds. During this process, we smooth the raw data using a Savitzky–Golay algorithm with a 7-point window to reduce the inherent pixel noise.

Figure 1(B) shows the chemical structure and absorbance of DTTC iodide. The shape of the absorption spectrum is in good agreement with that reported in the literature.[24] The wavelength of the Raman pump (800 nm) is located on the red side of the absorption peak (~760 nm), satisfying pre-resonance Raman conditions. Spectroscopic-grade DTTC was purchased from Radiant Dyes Laser Acc. GmbH and used without further purification. The tested concentrations, dissolved in dimethylsulfoxide (DMSO), ranged from 1×10^{-5} to 1×10^{-3} M; the spectra of the 5×10^{-4} M solution were selected to minimize the perturbation from the solvent. DTTC iodide is a near-infrared laser dye that efficiently emits light via STE and is frequently utilized for the fabrication of dye-nanoparticle conjugates.[25] Polymethines in DTTC dye are vulnerable to light exposure even in daylight, and as the DTTC iodide changes in colour from green to yellow after repeated experiments,[26] we performed each experiment with a fresh sample in a light-shielded atmosphere with low-energy pump (0.2–0.3 μJ/pulse) and probe (0.02–0.03 μJ/pulse) beams.

Generalized two-dimensional correlation spectroscopy (2DCOS) was employed to evaluate the vibrational components of the collected data. Details are given elsewhere,[27] but in brief, a Labview program written in-house based on the algorithm proposed by Noda and Ozaki[28] removes the background offsets from the fSRS spectra regardless of the optical perturbations.

3. RESULTS AND DISCUSSION

Prior to examining the resonance fSRS spectroscopy of DTTC iodide, we clarified the off-resonance fSRS spectroscopy of DMSO, which does not exhibit absorption near 800 nm (Fig. 2(A)). There was no overall discernible background over the spectral range considered; however, a wrinkle-shaped peak at around 670 cm^{-1} (C-S stretching) related to cross-phase modulation (XPM) appears for negative time delays (the probe beam precedes the pump beam; this feature is suppressed if the detection angle is increased.[29] The XPM artefacts gradually disappear as the time delay increases (a positive time delay indicates that the pump pulse arrives before the probe pulse), and there is a gradual increase in the intensities of the fSRS features until a delay time of zero (*i.e.*, synchronized pump and probe beams). The XPM signal has a duration of approximately 1 ps, which is shorter than the non-resonance CARS signal (1.5–2 ps) reported in the literature.[20]

Figure 2(B) compares the fSRS spectra of DMSO and DTTC iodide. Unlike the pure DMSO, the DTTC-iodide spectrum has a large background signal created by electronic absorption, as illustrated schematically in the insets. We also performed a spontaneous Raman scattering experiment using a single laser beam (cw; 785 and 514 nm) and found that the fluorescence background signals dominated the unrecognizable Raman signals (data not shown).

To verify the variation in the electronic gain/loss function (R_e) sustains an electronic resonance, we compared the time-integrated spectra of DMSO and DTTC iodide. Figure 3(A) shows the fSRS spectra of DMSO measured for a certain time delay (black) and that summed over a ~4-ps window (red). Since R_e is real, it must be zero in the non-resonance condition over time ($\int R_e \, dt_i = 0$);[30] this manifests as the excellent agreement between the signals for a specific time (black) and a short interval (red). If electronic resonance is present, then the Raman features in the fSRS spectra will be blurred by STE as in Fig. 3(B). To determine how long it takes for the STE to obscure the Raman signal, we integrated the DTTC-iodide fSRS spectra over various time-delay intervals up to a maximum time delay of 1 ns (Fig. 3(C)). We

found that the fSRS spectra are completely congested by ~10 ps and that the stimulated-emission signature was still present in the −0.8 to 1 ns integrated signal. The fitted lifetime (τ_0) of the STE retrieved from the intensity-time profile ($I = e^{-t/\tau_0}$) was approximately 50 ps, which is somewhat longer than the fluorescence decay times (~11 ps [31] and ~35 ps [32]) of DTTC iodide reported in the literature.

To examine the spectro-temporal features of the fSRS spectra in detail, we produced an fSRS spectrogram as a function of both the pump–probe delay and wavenumber. The 3D spectrogram in Fig. 4(A) reveals that there is a sharp increase in the fSRS intensity near 0 ps and that the background levels off with an increase in the time delay (up to 5 ps) especially at lower wavenumbers. The 2D colour plot gives a clearer picture of the spectral variation as a function of time. We see that we can obtain good temporal resolution for the vibrational states in the 'fingerprint region' between 1000 and 1600 cm^{-1} with a time delay of approximately 1.5–2 ps. We also see that there is a slight reduction in the spectral resolution if the centre wavelength of the probe is shifted from 890 nm to 920 nm.

Figure 4(B) shows the time-gated fSRS spectra of DTTC iodide obtained by taking profiles of the intensity between the orange and red dotted lines in Figure 4(A) every 0.2 ps. Each spectrum exhibits both SRS (sharp peaks) and STE (broad background) signals. Several noticeable Raman-resolved vibrations include CH_2 rocking (~780 cm^{-1}), C=C stretching (~840 cm^{-1}), and CH bending (~1240 cm^{-1}). The spectral resolution was measured to be ~27 cm^{-1}, which is comparable to our previous result.[33] The fSRS intensity can be seen to vary considerably with changes in the time delay, but profiling the variance of the Raman-only feature in the pump–probe cross correlation of the fSRS intensity shows that there are similarities for the on-(DTTC) and off-(DMSO) resonance conditions. The time evolution of the fSRS intensity reflects the convolution of the pump and probe pulses, and therefore, time traces of the fSRS will be influenced by pump-pulse elongation via the narrow bandpass filter

(NBPF), as detailed for different filters in our previous work.[33] The bandwidths of the fSRS spectra of DTTC iodide remain almost unchanged within the surveyed temporal range and are in agreement with the CARS case.[23] The lifetime of the SRG (CH-bending; ~1240 cm^{-1}) is compared with that of STE (~1650 cm^{-1}) in Figure 5(a);[‡] which shows that the SRG lifetime ranges from 1.5–2 ps, whereas that of the STE is ~50 ps, as mentioned earlier. Interestingly, the rise time of the STE is delayed by almost 0.5 ps; attenuated STE can be ascribed to the asymmetric pulse stretching towards the back end of the metal layer in the NBPF.

Background-free spectra are crucial for quantitative analysis, and inaccurate background correction processes will degrade the data in an arbitrarily weighted direction. Thus, we attempted to obtain a background-emission-free spectra using the time-gated approach hinted at in the data in Fig. 5(A). For reference, we also obtained an unweighted background-suppressed spectrum using 2DCOS. Figure 5(B) compares the fSRS spectra obtained with the 2DCOS method and those recorded for the probe delays 1 and 2 indicated in Figure 5(A). 2DCOS analysis is known to be a powerful tool for analysing signals with different trends (here, the increase in the STE and the decay in the fSRS), and the slicing spectrum of the resulting asynchronous spectra of 2DCOS represents a background-corrected spectrum. Spectrum 2 is obtained for almost fully overlapped pump and probe beams, and we see that the scattering efficiency around 1240 cm^{-1} is more than 40% of that of the total intensity at maximum overlap. Spectrum 1, in contrast, is recorded for a time delay of −0.2 ps and shows Raman bands near 1400 cm^{-1} that are better resolved than those in spectrum 2. In addition, the background emission is almost zero, but the signal-to-noise ratio has been reduced.

There have been a number of quantum mechanical studies[6] of fSRS phenomena and a recent study using perturbation theory,[34] the results of which were successfully reproduced in a subsequent experiment.[16] According to these studies; virtual states in the stimulated Raman

process mediate the coherent scattering, while real states with the finite radiation states mediate the STE. If we assume here that electron propagation towards the real excited state is tailored because the pump energy (1.55 eV) was lower than the absorption (1.64 eV) of DTTC iodide, then the electron propagation will also disturb the escalation of coherent electronic emission and allow vibrational coherent scattering (*i.e.*, SRS) to occur before STE. This 'time-wise' trend is likely to be reversed once the pump and probe beams are overlapped. Therefore, in the early stages of pump–probe overlap, electronic build-up to the excited state is still taking place and only the relatively stronger occurrence of stimulated Raman scattering is permitted.

4. CONCLUSION

In summary, we have successfully achieved highly background-suppressed fSRS spectroscopy using the time-gated approach. SRG spectra of DTTC iodide were obtained using a computational algorithm and a pulse stabilization method, which yielded a good signal-to-noise ratio. The performance of the fSRS spectroscopy was verified by surveying fSRS spectra of DMSO, for which we confirmed the appearance of low-intensity XPM-induced signals in the early stages of beam mixing. Temporal panoramic fSRS spectra of DTTC iodide revealed the time evolution of the SRG and STE profiles, showing the feasibility of background elimination. The best background-free spectral profiles were obtained when the probe beam was delivered to the molecules in advance of the pump beam by ~0.2 ps. We believe that substantial background suppression can be mainly ascribed to the difference in the SRS and STE lifetimes. Based on the results presented here, we intend to use oscillator-based fSRS spectroscopy to study the effects of higher-frequency modulation to compensate for the weak signal-to-noise level in the time-gated measurement. It will also

be intriguing to determine whether shorter pulses will improve the time resolution and to examine the effects of different pump wavelengths.

ACKNOWLEDGEMENTS

Y.D.S. was supported by KRICT (SI-1308, KK-0904-02, OASIS Project), the Nano R&D Program (No. 2009-0082861). SMJ and YDS also acknowledge the financial support from the Industrial Strategic Technology Development Program (nos. 10033183 and 10037397) funded by the Ministry of Trade, Industry, and Energy (MI, Korea), and Infopia Co., Ltd. (II-0904). This research was also supported by the Public welfare & Safety research program (2011-0020957) and by Basic Science Research Program (NRF-2013R1A1A1008710) through the National Research Foundation of Korea funded by the Ministry of Education. HK acknowledges the provision of DGIST basic research program (14-NB-04) for preparing the manuscript.

FIGURE CAPTIONS

Fig. 1 (A) Schematic diagram of the fSRS system. BS: beam splitter; CF: colour filter; CM: concave mirror; HRR: horizontal retro-reflector; IR: iris; NBPF: narrow band pass filter; NF: notch filter; PL: planoconvex lens; SP: sapphire plate; PP: Raman pump; Pr: Raman probe; rf: reference beam. (B) Absorption spectrum of DTTC iodide. The wavelengths of the pump (800 nm) and probe (890 nm at the centre position) beams are also indicated.

Fig. 2 (A) Time-gated fSRS spectra of DMSO for various pump–probe time delays. (B) Comparison of the fSRS spectra of DTTC diode (black line) and DMSO (red line). Insets

depict molecular energy diagrams for the non-resonance (DMSO) and pre-resonance (DTTC) conditions with respect to the excitation beams.

Fig. 3 The fSRS spectra of (A) DMSO and (B) DTTC iodide for time-integrated (red) and single-time (black) collections. (C) Time-integrated fSRS spectra for various time-delay intervals.

Fig. 4 (A) The fSRS intensity as a function of the time delay (ps) and wavenumber (cm^{-1}) shown on a 2D colour scale and as a 3D spectrogram to give a better description of the spectral morphology. (B) A waterfall display of the fSRS spectra from −0.6 ps (dotted orange line) to 1.4 ps (dotted red line). The interval between each spectrum is 0.2 ps.

Fig. 5 (A) Time profiles of the fSRS spectra for the STE (black dots; ~1640 cm^{-1}) and SRG (red dots; ~1240 cm^{-1}). The inset energy diagram shows the time delay (τ) between the pump (red) and probe (grey) pulses. The dotted red arrow indicates the resonance energy (1.64 eV) of DTTC, while the solid red arrow indicates the excitation energy (1.55 eV) used in this work. (B) Comparison of the background-subtracted spectrum (2DCOS) and time-gated fSRS spectra (1, 2) of DTTC iodide recorded at the pump–probe delays indicated in (A).

NOTES AND REFERENCES

‡ We chose 1650 cm^{-1} as the position to measure the stimulated emission because of the difficulty in separating the STE from the SRG in the fingerprint region (1000–1500 cm^{-1}).

1 B. G. Saar, C. W. Freudiger, J. Reichman, C. M. Stanley, G. R. Holtom and X. S. Xie, *Science*, 2010, **330**, 1368–1370.

2 G. Eckhardt, R. W. Hellwarth, F. J. McClung, S. E. Schwarz, D. Weiner and E. J. Woodbury, *Phys. Rev. Lett.*, 1962, **9**, 455–457.

3 N. Bloembergen and Y. R. Shen, *Phys. Rev. Lett.*, 1964, **12**, 504–507.

4 Y. R. Shen and N. Bloembergen, *Phys. Rev.*, 1965, **137**, A1787–A1805.

5 D. W. McCamant, P. Kukura and R. A. Mathies, *Appl. Spectrosc.*, 2003, **57**, 1317–1323.

6 P. Kukura, D. W. McCamant and R. A. Mathies, *Annu. Rev. Phys. Chem.*, 2007, **58**, 461–488.

7 P. Kukura, R. Frontiera and R. A. Mathies, *Phys. Rev. Lett.*, 2006, **96**, 238303.

8 P. Kukura, D. W. McCamant, P. H. Davis and R. A. Mathies, *Chem. Phys. Lett.*, 2003, **382**, 81–86.

9 P. Kukura, D. W. McCamant, S. Yoon, D. B. Wandschneider and R. A. Mathies, *Science*, 2005, **310**, 1006–1009.

10 S. Y. Lee and E. J. Heller, *J. Chem. Phys.*, 1979, **71**, 4777–4788.

11 R. S. Chao, R. K. Khanna and E. R. Lippincott, *J. Raman Spectrosc.*, 1975, **3**, 121–131.

12 D. B. Chase, *J. Am. Chem. Soc.*, 1986, **108**, 7485–7488.

13 G. W. Chantry, H. A. Gebbie and C. Hilsum, *Nature*, 1964, **203**, 1052–1053.

14 P. Matousek, M. Towrie and A. W. Parker, *J. Raman Spectrosc.*, 2002, **33**, 238–242.

15 A. P. Shreve, N. J. Cherepy and R. A. Mathies, *Appl. Spectrosc.*, 1992, **46**, 707–.

16 R. R. Frontiera, S. Shim and R. A. Mathies, *J. Chem. Phys.*, 2008, **129**, 064507.

17 R. W. Boyd, *Nonlinear Optics*, Academic Press, San Diego, 2003.

18 G. Vicidomini, G. Moneron, K. Y. Han, V. Westphal, H. Ta, M. Reuss, J. Engelhardt, C. Eggeling and S. W. Hell, *Nat. Methods*, 2011, **8**, 571–573.

19 J. R. Moffitt, C. Osseforth and J. Michaelis, *Opt. Expr.*, 2011, **19**, 4242–4254.

20 F. Ganikhanov, C. L. Evans, B. G. Saar and X. S. Xie, *Opt. Lett.*, 2006, **31**, 1872–1874.

21 C. L. Evans, E. O. Potma and X. S. Xie, *Opt. Lett.*, 2004, **29**, 2923–2925.

22 D. Pestov, G. O. Ariunbold, X. Wang, R. K. Murawski, V. A. Sautenkov, A. V. Sokolov and M. O. Scully, *Opt. Lett.*, 2007, **32**, 1725–1727.

23 D. Pestov, R. K. Murawski, G. O. Ariunbold, X. Wang, M. Zhi, A. V. Sokolov, V. A. Sautenkov, Y. V. Rostovtsev, A. Dogariu, Y. Huang and M. O. Scully, *Science*, 2007, **316**, 265–268.

24 P. P. Sorokin, J. R. Lankard, E. C. Hammond and V. L. Moruzzi, *IBM J. Res. Dev.*, 1967, **11**, 130–148.

25 M. V. Yigit, L. Zhu, M. A. Ifediba, Y. Zhang, K. Carr, A. Moore and Z. Medarova, *ACS Nano*, 2011, **5**, 1056–1066.

26 Y. Miyazoe and M. Maeda, *Opt. Quantum Electron,* 1970, **2**, 227–233.

27 H. M. Kim, H. S. Park, S. M. Jin, K. T. Lee, Y. M. Jung and Y. D. Suh, submitted.

28 I. Noda and Y. Ozaki, *Two-Dimensional Correlation Spectroscopy: Applications in Vibrational and Optical Spectroscopy*, Wiley, Chichester, 2004.

29 K. Ekvall, P. van der Meulen, C. Dhollande, L.-E. Berg, S. Pommeret, R. Naskrecki, and J.-C. Mialocq, *J. Appl. Phys.*, 2000, **87**, 2340–2352.

30 S. A. Kovalenko, A. L. Dobryakov, J. Ruthmann and N. P. Ernsting, *Phys. Rev. A*, 1999, **59**, 2369–2384.

31 K. Kasatani and H. Sato, *Bull. Chem. Soc. Jpn.*, 1996, **69**, 3455–3460.

32 H. Tashiro and T. Yajima, *Chem. Phys. Lett.*, 1976, **42**, 553–557.

33 S. M. Jin, Y. J. Lee, J. W. Yu, and S. K. Kim, *Bull. Korean Chem. Soc.*, 2004, **25**, 1829–1832.

34 Z. Sun, J. Lu, D. H. Zhang, and S.-Y. Lee, *J. Chem. Phys.*, 2008, **128**, 144114.

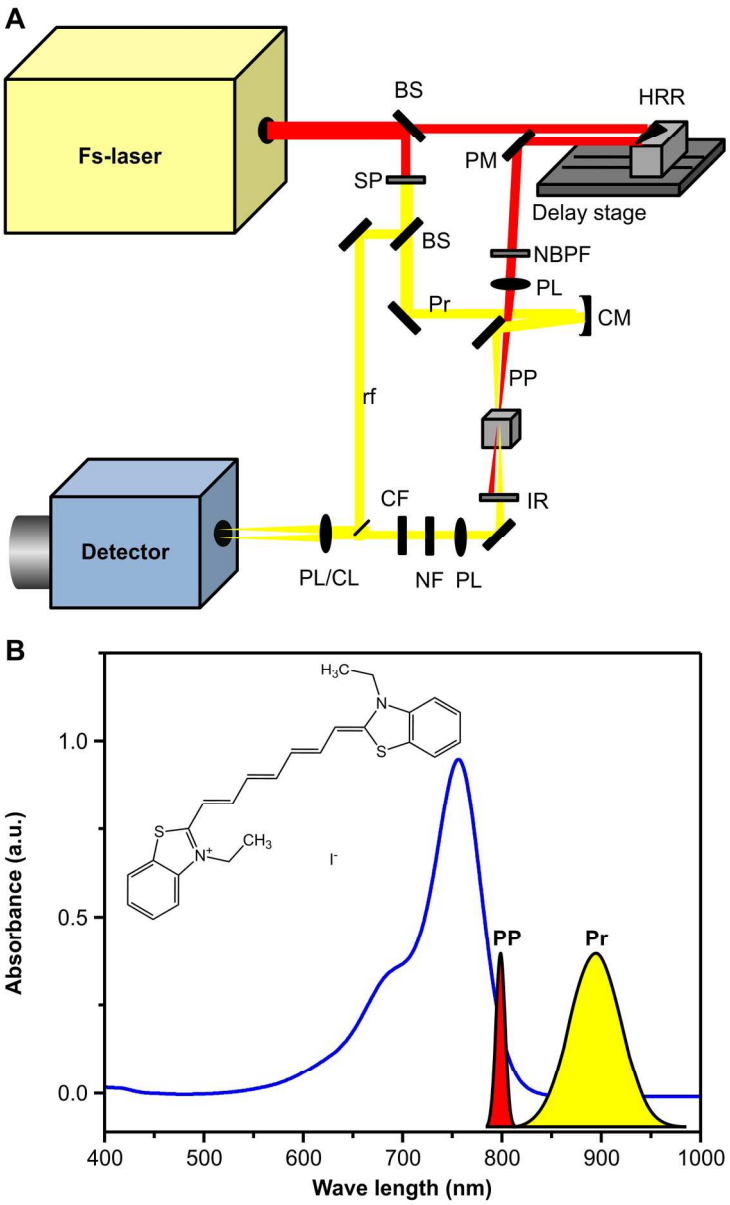

136x226mm (300 x 300 DPI)

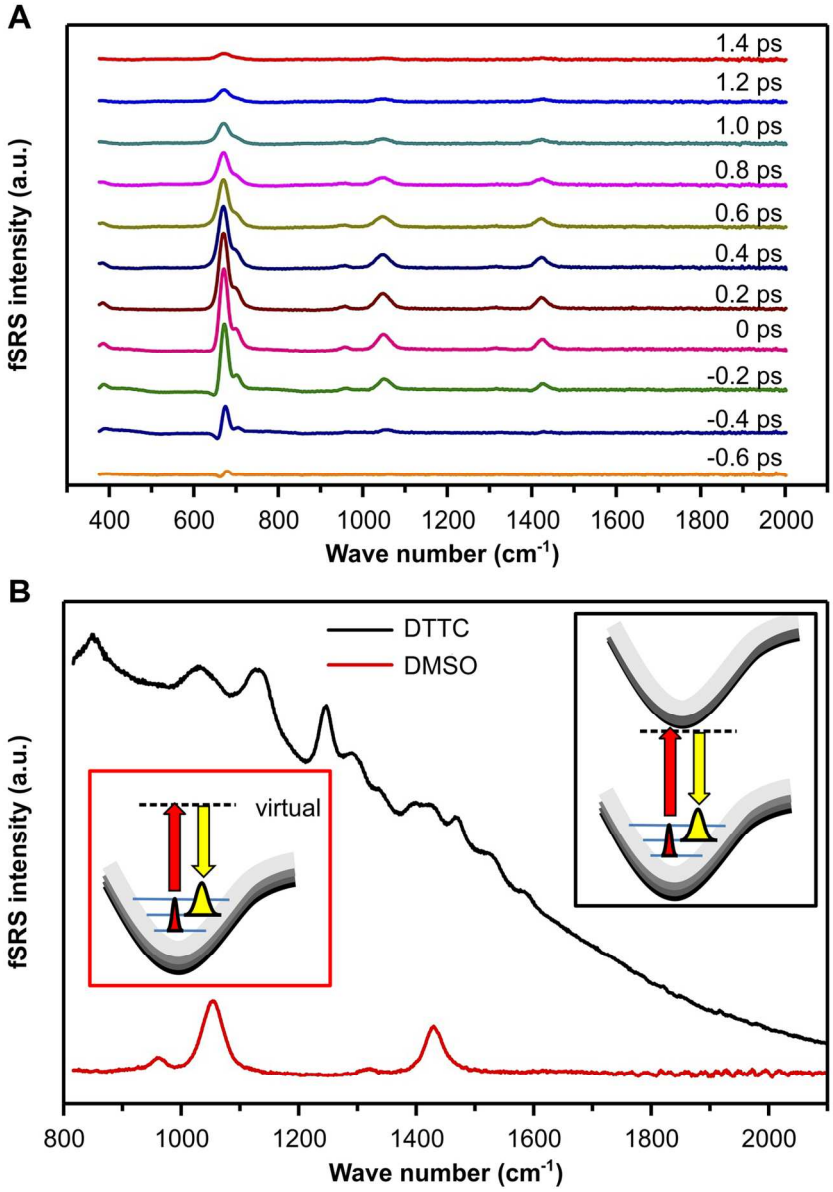

119x173mm (300 x 300 DPI)

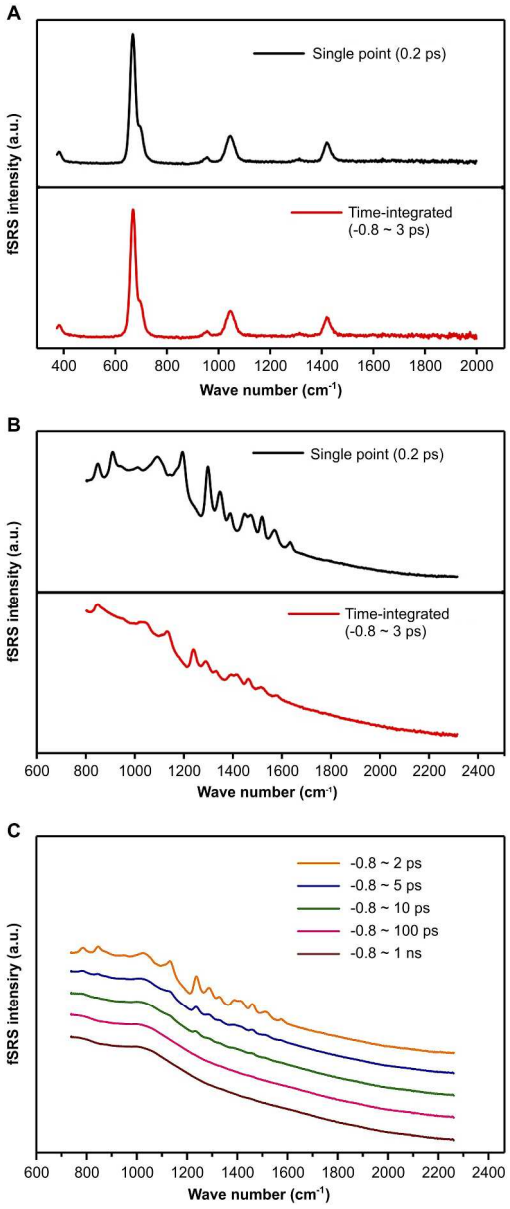

197x472mm (300 x 300 DPI)

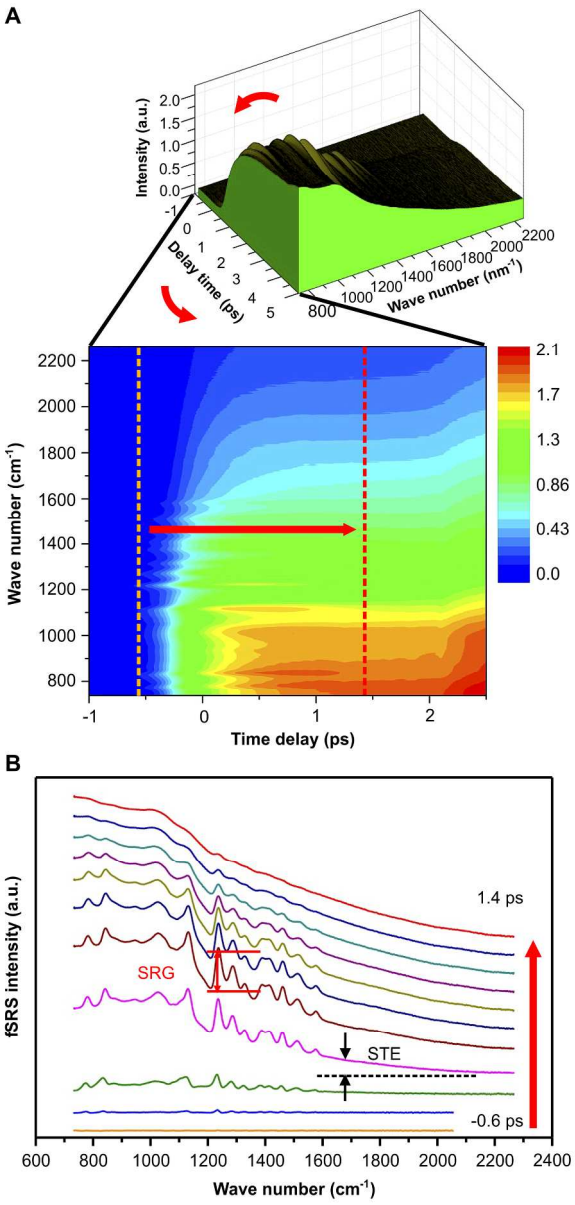

172x360mm (300 x 300 DPI)

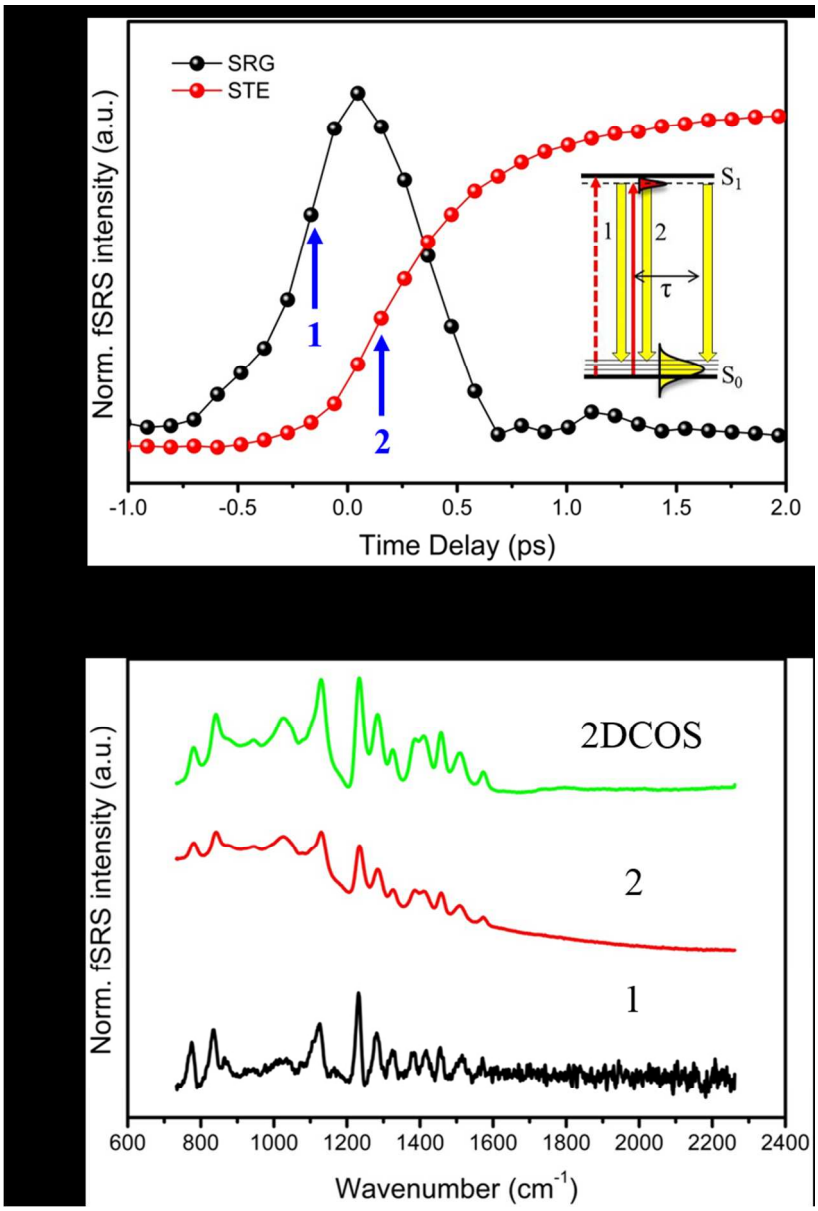

148x219mm (150 x 150 DPI)

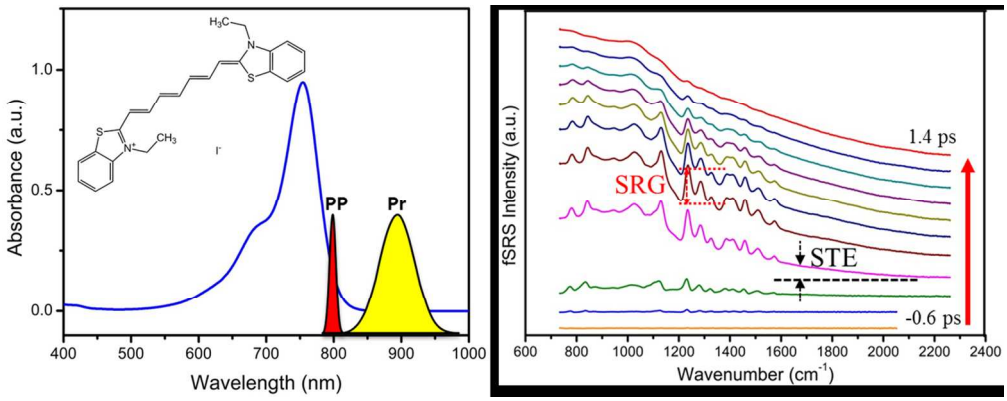

240x93mm (150 x 150 DPI)